The 20th International Flow Measurement Conference FLOMEKO 2026

Non-Intrusive Analytic Temperature Model for Rate-of-Rise Gas Flow Standards

A. N. Johnson[1*], J. G. Pope[1]
K. A. Gillis[1], J. D. Wright[1], and C. J. Crowley[1]

1 National Institute of Standards and Technology, 100 Bureau Dr, Gaithersburg, MD, 20899, USA
* E-mail: Aaron.Johnson@nist.gov

Abstract

Accurate measurement of low gas flows is essential in semiconductor manufacturing because mass flow controllers (MFCs) regulate gas stoichiometry during critical processes such as etching and deposition, which directly affect device performance and yield. The *R*ate-of-*R*ise (*RoR*) method, widely used for MFC calibration, determines mass flow rate by introducing steady gas flow into a vessel of known volume and measuring the resulting increase in gas density. However, compression heating during filling generates a transient, non-uniform temperature field. Errors in temperature measurement propagate to density and, consequently, mass flow rate. We propose a novel *RoR* collection vessel geometry with a long, slender, thermostatted tube that simplifies heat transfer, enabling an analytical solution for gas temperature. Our model, which was validated for five gases (Xe, SF_6, CO_2, N_2, Ar), predicts the steady-state average gas temperature with a standard uncertainty of 37.5 mK, relying only on wall temperature and gas pressure measurements. Using a long, slender collection vessel and the accompanying thermal model will enhance the accuracy of *RoR* flow standards and support reliable, SI-traceable MFC calibration.

1. Introduction

In semiconductor manufacturing, mass flow controllers (MFCs) regulate individual process gas flows to control process stoichiometry and chamber pressure during deposition and etching. At flow rates below 1000 sccm (standard cubic centimeters per minute [1]), calibration accuracy becomes a dominant contributor to overall measurement uncertainty, particularly for hazardous gases [1]. The Rate-of-Rise (*RoR*) calibration method, widely adopted by industry for its operational robustness, determines mass flow by measuring the rate of density increase in a fixed-volume collection vessel as it fills [2]. However, compression heating during filling produces spatially and temporally varying temperature fields that complicate accurate density determination, and thereby mass flow determination [3]. These effects have not been adequately quantified in the limited *RoR* literature.

Industry *RoR* standards often assume that the gas temperature in the collection vessel is constant during filling. Alternatively, they rely on direct measurement of the gas temperature, which is subject to well-known challenges: slow sensor response, limited spatial resolution, self-heating biases, and incompatibility with corrosive gases. Errors in temperature measurement directly propagate into density errors, ultimately affecting the mass flow rate and limiting the applicability of the *RoR* method across gas species and operating conditions. Zhang et al. (2024) highlighted the importance of reliable physical models to account for temperature and other factors affecting flow standards in semiconductor applications [4]. We present a novel collection vessel design that ensures radial conduction dominates heat transfer. As a result, a simple, physics-based thermal model can be used to account for flow work and accurately estimate the average gas temperature from exterior wall measurements throughout the filling period.

This manuscript complements our earlier work [5], which introduced NIST's *RoR* Semiconductor Low Flow Standard (SLowFlowS). That work described the standard's design, including a collection vessel in a thermostatted enclosure with a wall temperature held constant and selectable between 20°C and 26°C. The standard achieves an SI-traceable flow range of 0.01 sccm to 1000 sccm with expanded uncertainties as low as 0.06 %. We experimentally validated the thermal model for SF_6 and N_2 in the previous work, but the theoretical basis was not reported. This study derives the thermal model rigorously, establishes a full energy balance, and examines transient and steady-state behavior of the gas in the vessel during filling. We extend the experimental validation to Xe, CO_2, and He. Xenon represents the design-limiting case due to its extremely low thermal conductivity, while CO_2 and He demonstrate applicability across a range of thermal properties.

[1] The unit sccm is standard cubic centimeters per minute where the standard volumetric flow Q_{std} is obtained by dividing the mass flow rate $\dot{m}$ by the reference gas density, assuming ideal-gas behavior at the standard conditions T_{std} = 273.15 K and P_{std} = 101.325 kPa.

2. Collection Vessel Design

Figure 1 illustrates a typical *RoR* setup used to calibrate a MFC. The novelty of this setup lies in the use of a long, slender collection vessel housed in a thermostatted enclosure and equipped with surface-mounted temperature sensors and pressure transducers. The calibration process begins with the tank inlet valve open and the valve to the vacuum pump closed. The MFC delivers a steady mass flow into the initially evacuated collection vessel of known volume V. Simultaneously, the back-pressure regulator (BPR) maintains a constant pressure at the MFC's outlet as the vessel pressure rises. For a constant mass flow rate $\dot{m}$ into the vessel, the rate of mass accumulation is constant, leading to a linear increase in gas density with time. The mass flow rate, $\dot{m}$, is calculated as the product of the vessel volume and the slope of a linear regression of the measured density versus time.

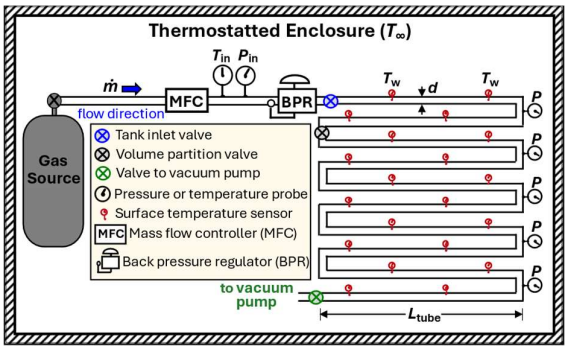

Figure 1. Typical *RoR* calibration setup: gas source, mass flow controller (MFC), back-pressure regulator (BPR), and valves feeding into a novel long, slender collection tube of known volume separated into two sections by a partition valve, all housed in a thermostatted enclosure at constant wall temperature $T_w = T_\infty$.

While conventional *RoR* collection vessels often have a short, wide geometry, such as spheres or cylinders with hemispherical ends, we employ a long slender cylindrical tube illustrated in **Figure 1**. This geometry simplifies heat transfer and results in a predictable internal temperature profile during filling. We realize this design in our NIST *RoR* standard, SLowFlowS, using an internal diameter of $d = 2\,R_i = 1.143$ cm. Two fill lengths are implemented within the same tube: a shorter segment, referred to as the two-tube vessel, with an aspect ratio $L/d = 320$, and a longer segment, referred to as the sixteen-tube vessel, with an aspect ratio $L/d = 2560$ (see Reference [5] for details). The two-tube vessel extends from the back-pressure regulator (BPR) to the volume partition valve, providing a smaller volume that enables efficient low-flow measurements (0.01 sccm to 125 sccm). The sixteen-tube vessel includes the full tube up to the valve used for evacuation (vacuum pump valve), accommodating higher flows (0.1 sccm to 1000 sccm). Here, L denotes the total length of the collection path, including the straight tube sections (L_{tube} in **Figure 1**) and the lengths of the U-bend elbows.

These high-aspect-ratio geometries are selected such that radial conduction dominates heat transfer during filling, minimizing contributions from natural and forced convection. The vessel's small diameter and horizontal orientation suppress buoyancy-driven flows, while the closed end and low flow rates render axial forced convection negligible. Under these conditions, the gas thermal response is predictable and primarily governed by radial conduction through the vessel wall, which underpins the assumptions used in the mathematical model in Section 3.

To quantify the thermal response during filling, we define a dimensionless thermal response factor, ε, as the ratio of the compression (flow-work) heating to radial conductive heat loss,

$$\varepsilon = \frac{\dot{m} N_R R_g}{8\pi k L}. \qquad (1)$$

The thermal response factor, ε, represents the combined influence of vessel geometry, gas properties, and mass flow on the temperature increase due to flow work. Specifically,

- A longer vessel length L provides more surface area for radial heat loss.
- Higher gas thermal conductivity k enhances radial conduction.
- Lower mass flow rate $\dot{m}$ reduces compression heating.
- Gas properties: a higher specific gas constant $R_g = R_u/\mathcal{M}$ (where R_u is the universal gas constant and $\mathcal{M}$ is the gas molar mass), or significant real-gas effects (represented by the real-gas responsivity factor N_R) can enhance or modify compression heating. These effects are discussed in Section 3.

Collectively, these parameters are chosen to keep $\varepsilon \ll 1$, so that the gas temperature remains close to the wall temperature T_w. The primary design parameter is the vessel length L, which is selected during vessel design to maintain a small ε even for the lowest-conductivity gases at the highest flow rates, thereby keeping temperature rise small across all gases and operating conditions. For the two SLowFlowS collection vessels, with maximum flows of 125 sccm and 1000 sccm, respectively, the design limit thermal response factor is $\varepsilon_{max} = 0.00153$, set by xenon, the lowest-conductivity gas. The maximum flow of 125 sccm strictly applies to xenon but is conservatively adopted for other gases with higher thermal conductivities.

A small ε also ensures that the volume-averaged gas temperature $T(t)$ rapidly approaches steady-state with a predictable temperature rise. The quasi-steady-state gas temperature is

$$T_{ss} = \frac{T_w}{1-\varepsilon}. \qquad (2)$$

The fractional temperature increase satisfies $\Delta T/T_{ss} = \varepsilon$, where the temperature increase attributed to flow work is $\Delta T = T_{ss} - T_w$.

The analytical model presented in Section 3 predicts the transient temperature evolution, $T(t)$, which rapidly approaches the quasi-steady-state temperature, T_{ss}, where radial conductive heat loss through the vessel wall balances the thermal energy input from flow work**.** The time scale to reach steady-state can be computed, allowing mass determination to begin only once the gas is effectively at T_{ss}, enabling high-fidelity density determinations. The model couples mass conservation, energy conservation, and the equation of state, which provides the basis for non-intrusive mass flow measurements from the measured wall temperature and pressure.

3. Mathematical Model for Average Gas Temperature

We develop a reduced-order model to predict the volume-averaged gas temperature, $T(t)$, within the long, slender collection vessel shown in **Figure 1**. The vessel has a small diameter, a high aspect ratio, and is oriented

horizontally. Under the operating conditions described in Section 2, heat transfer is primarily by radial conduction, while axial conduction and buoyancy-driven natural convection are negligible. Accordingly, we obtain the volume-averaged gas temperature $T(t)$ by first determining the radial temperature distribution $\hat{T}(r,t)$ and then integrating it over the vessel volume,

$$T(t) = \frac{1}{V}\int_V \hat{T}(r,t)dV = \frac{1}{\pi R_i^2}\int_0^{R_i} \hat{T}(r,t)2\pi r dr \,. \qquad (3a)$$

During the filling process, compression heating produces a temperature $\hat{T}(r,t)$ that decreases monotonically from the vessel's centerline. For the operating conditions considered, the temporal increase in the volume-averaged gas temperature is small ($\Delta T/T_{ss} \ll 1$), where $\Delta T = T_{ss} - T_w$ represents the temperature change from the initial state, when the gas is in thermal equilibrium with the wall at T_w, until reaching the quasi-steady-state temperature, T_{ss}. As a result, the volume-averaged temperature is only weakly sensitive to the exact shape of the radial profile. This insight enables us to select a profile that simplifies the analysis while retaining the essential physics.

We model the radial temperature distribution by a power-law form, which provides a compact representation of a monotonically decreasing profile while keeping the analysis analytically tractable. The profile is,

$$\begin{aligned} \hat{T}(r,t) &= \hat{T}(0,t) + (T_w - T_0(t))\left(r/R_i\right)^n , \\ \hat{T}(0,t) &= \left((n+2)T(t) - 2T_w\right)/n , \end{aligned} \qquad (3b)$$

where, $n \geq 1$ is the exponent controlling the shape of the temperature profile $\hat{T}(r,t)$, T_w is the measured vessel wall temperature, R_i is the inner radius, and $\hat{T}(0,t)$ is the instantaneous temperature along the vessel axis. The expression for $\hat{T}(0,t)$ in Equation (3b) ensures that the volume-average of $\hat{T}(r,t)$ is consistent with $T(t)$ from Equation (3a).

Although the filling process is globally transient, the radial temperature profile may be treated as quasi-steady. Radial conduction redistributes thermal energy more rapidly than if it is generated locally by compression heating, so the spatial structure of the temperature field is analogous to steady-state conduction with uniform volumetric heat generation. In this reference case, the balance produces a parabolic temperature distribution with a maximum at the centerline and zero radial gradient at $r = 0$ [6].

For our case of gas filling a cylindrical vessel, the situation is slightly more complex: the mass and temperature are transient, and the compression heating depends on the local temperature, making the heat generation slightly nonuniform. Nevertheless, the small-ε design ensures that the local temperature rises are small compared with the absolute temperature. Under these conditions, the heat generation may be treated as approximately uniform, and the radial temperature profile rapidly approaches a shape closely resembling the parabolic reference profile [6]. Moreover, because the inflowing gas has nearly the same enthalpy as the gas already in the vessel, the transient effects do not significantly distort the profile.

These considerations justify approximating the radial temperature profile as parabolic, even during the transient filling process. This motivates the choice of $n = 2$ as the baseline exponent in the generalized power-law profile of Equation (3b). For clarity and generality, the symbol n will be retained in the energy balance equations until the parabolic case is explicitly applied.

Section 3.1: Mass Conservation

Mass conservation requires that the rate of change of gas mass within the vessel equals the inflow rate. For a constant mass flow rate, the gas mass evolves as

$$m(t) = m_i + \dot{m}\, t \,, \qquad (4)$$

so that the volume-averaged density is $\rho(t) = m(t)/V$, defined as the gas mass divided by the interior vessel volume V.

Section 3.2: Energy Balance

The energy balance for the gas in the vessel can be expressed in terms of temperature as

$$mc_V \frac{dT}{dt} = -Q_{out} + \dot{m}N_R R_g T + \dot{m}(h_{in} - h) \,, \qquad (5)$$

where $h = e + P/\rho$ is the specific enthalpy of the gas in the vessel, e is the internal energy of the gas, h_{in} is the specific enthalpy of the inflowing gas, c_V is the constant-volume specific heat, Q_{out} is the conduction heat transfer rate to the vessel walls, and

$$N_R = Z\frac{T\beta}{P\kappa_T} \,, \qquad (6)$$

is the real-gas responsivity factor. The factor N_R accounts for compressibility and other non-ideal effects, scaling the contribution of compression (flow work) relative to an ideal gas, for which $N_R = 1$. Here, Z is the compressibility factor, β is the gas volume expansivity, and κ_T is the isothermal compressibility.

Neglecting enthalpy term in the energy balance

When the inlet gas temperature T_{in} is close to the wall temperature T_w, the enthalpy term $\dot{m}(h_{in} - h)$ in Equation (5) is small relative to the compression (flow work) term $\dot{m}N_R R_g T$ and can be neglected. For illustration, consider an ideal gas, where the constant-pressure specific heat is $c_P = R_g\gamma/(\gamma - 1)$ with $\gamma = c_P/c_V$. The enthalpy term reduces to $\dot{m}\, c_P(T_w - T)$ and the flow work term simplifies to $\dot{m}\, R_g T$.

In the steady-state limit, the ratio of the enthalpy term to flow work term is significantly less than unity,

$$\frac{c_p(T_w - T_{ss})}{R_g T_{ss}} = \left(\frac{\gamma}{\gamma - 1}\right)\left(\frac{T_w - T_{ss}}{T_{ss}}\right) = \frac{-\gamma\varepsilon}{\gamma - 1} << 1 \,. \qquad (7)$$

Here, $\varepsilon = -(T_w - T_{ss})/T_{ss}$ is the thermal response factor, which is, by design, significantly less than unity. For the conditions considered in this work, the enthalpy term is negligible and is therefore omitted in the subsequent analysis.

Conductive heat transfer with general n

The conductive heat transfer to the lateral wall is given by

$$Q_{out} = \int_S q'' dS = \int_0^L -k\left.\frac{\partial \hat{T}}{\partial r}\right|_{R_i} 2\pi R_i dz \,, \qquad (8a)$$

where k is the gas thermal conductivity, q'' is the heat flux, and S is the lateral surface. End effects are neglected due to the high aspect ratio of the vessel. Using the generalized power-law profile from Equation (3b), the radial derivative at the wall is

$$\left.\frac{\partial \hat{T}}{\partial r}\right|_{R_i} = \frac{n\left(T_w - \hat{T}(0,t)\right)}{R_i} \,. \qquad (8b)$$

Carrying out the integration over the vessel length L results in the closed-form expression

$$Q_{\text{out}} = 2(n+2)\pi kL\left(T_{\text{w}} - T(t)\right). \tag{8c}$$

Specialization to parabolic profile ($n = 2$)
For the parabolic profile ($n = 2$), Equation (8c) simplifies to

$$Q_{\text{out}} = 8\pi kL\left(T_{\text{w}} - T(t)\right). \tag{9}$$

The temperature-based energy balance in Equation (5) including the expression for Q_{out} is

$$mc_{\text{V}}\frac{\text{d}T}{\text{d}t} = -8\pi kL\left(T_{\text{w}} - T(t)\right) + \dot{m}N_{\text{R}}R_{\text{g}}T. \tag{10a}$$

Normalized thermal response differential equation
The normalized form of Equation (10a) is

$$\left(\frac{(m_{\text{i}} + \dot{m}t)c_{\text{V}}}{8\pi kL}\right)\frac{\text{d}T}{\text{d}t} + (1-\varepsilon)T = T_{\text{w}}, \tag{10b}$$

where Equation (10a) has been divided by the characteristic conductance scale $8\,\pi\,k\,L$, and Equation (4) has been substituted for $m(t)$.

Normalizing the energy balance introduces the thermal response factor ε, which quantifies the relative importance of flow work heating compared with radial conduction:

$$\varepsilon = \frac{\dot{m}N_{\text{R}}R_{\text{g}}}{8\pi kL} = \frac{Q_{\text{std}}N_{\text{R}}P_{\text{std}}}{8\pi k\,LT_{\text{std}}}. \tag{10c}$$

The factor ε determines how strongly the gas temperature deviates from the wall temperature T_{w} during filling. It is used to predict both the quasi-steady-state temperature and the transient response, linking the vessel geometry, gas properties, and mass flow $\dot{m}$ (or standard volumetric flow Q_{std} defined in Footnote 1) to the expected thermal behavior. Readers are referred to Section 2 for a discussion of how ε informs vessel design.

Section 3.3: **Volume-Averaged Temperature Evolution**
To solve Equation (10b), the *Normalized Thermal Response Differential Equation*, we consider two stages of the *RoR* measurement, filling and final equilibration. Initially, the collection vessel is evacuated, with both the inlet and vacuum pump valves (**Figure 1**) closed, while the vessel walls and any residual low-pressure gas inside are maintained at the thermostatted temperature T_{w}, establishing the initial condition $T_{\text{i}} \approx T_{\text{w}}$.
Stage 1: Temperature evolution during filling ($\dot{m} \neq 0$)
During filling, the mass flow into the collection vessel is constant, and the gas temperature increases due to the opposing effects of compression (flow work) and radial conduction to the vessel walls. Under these conditions, Equation (10b) admits an analytical solution for the volume-averaged gas temperature,

$$T(t) = T_{\text{ss}} + \left(T_{\text{i}} - T_{\text{ss}}\right)\left(1 + \frac{t}{\tau_{\text{i}}}\right)^{-N}, \tag{11a}$$

where T_{i} is the initial gas temperature, the steady-state temperature is given by Equation (2), the exponent is

$$N = N_{\text{R}}\left(\frac{1-\varepsilon}{\varepsilon}\right)\frac{R_{\text{g}}}{c_{\text{V}}}, \tag{11b}$$

and the characteristic filling time is

$$\tau_{\text{i}} = \frac{m_{\text{i}}}{\dot{m}}. \tag{11c}$$

Together, τ_{i} and N govern the transient evolution toward T_{ss}, with smaller τ_{i} accelerating the approach to steady-state and larger N reducing the time required to reach T_{ss}. Because Q_{std} (or $\dot{m}$) is the measured flow and the gas properties (*e.g.*, k, R_{g}, c_{V}) cannot be adjusted as control parameters, τ_{i} can be decreased only by reducing the initial gas mass m_{i} in the collection vessel prior to filling, and N can be increased only by decreasing ε by designing a longer L collection vessel, as discussed in Section 2.

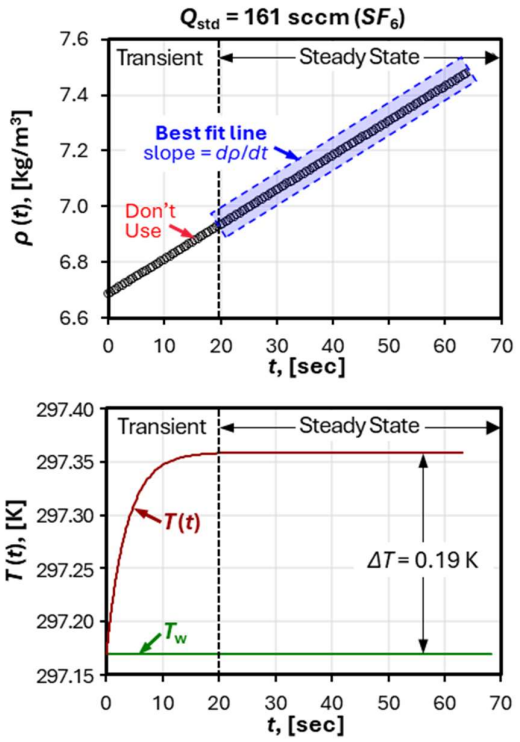

Figure. 2. Time evolution of gas density (upper panel) and temperature rise (lower panel) during filling of collection vessel with SF_6 at Q_{std} = 161 sccm. The temperature exhibits a transient increase due to compression heating before reaching a steady-state value T_{ss} approximately 0.19 K above the wall temperature T_{w}.

This analytical solution captures both the magnitude and time evolution of compression heating and enables accurate prediction of the transient and steady-state behavior in slender, collection vessels. The predicted steady-state temperature increase relative to the wall temperature is

$$\Delta T = T_{\text{ss}} - T_{\text{w}} = \frac{\varepsilon T_{\text{w}}}{1-\varepsilon}, \tag{12}$$

indicating that a small thermal response factor maintains the gas temperature close to the wall temperature.

Figure 2 shows the density as a function of time in the upper panel and the temperature rise during filling in the lower panel for SF_6 gas flowing at Q_{std} = 161 sccm. The temperature undergoes a transient increase lasting approximately 20 s before stabilizing at a steady-state temperature T_{ss}, which is roughly 0.19 K above the wall temperature, T_{w}**.** In conventional analyses that assume the gas temperature remains constant at the wall temperature T_{w}, the transient period is included in the mass flow calculation, resulting in a temperature-related error of roughly 0.5 % in the example of Figure 2.

Figure 2 was produced using a prototype tube design prior to establishing the SLowFlowS standard. This prototype configuration consisted of two tubes in parallel, each with an inner diameter of 2.1 cm and a length of 1.91 m, corresponding to a thermal response factor ε = 0.00085. At Q_{std} = 161 sccm of SF_6, the gas temperature required approximately 20 s to approach the steady-state value T_{ss}. According to Equation (11c), the characteristic filling time scales as $\tau_i \propto m_i/\dot{m}$; therefore, reducing the initial gas mass decreases τ_i and shortens the transient duration. The data shown in Figure 2 correspond to an initial gas mass of m_i = 8.758 g. For the same flow rate (Q_{std} = 161 sccm), we reduced the initial gas mass to m_i = 0.85 g by lowering the starting pressure and using a smaller-diameter tube of the same length. Under these conditions, the same steady-state temperature was reached in approximately 2 s.

The model's ability to capture and quantify this transient is a key advantage. By identifying the transient period and using T_{ss} instead of T_w, while excluding density data collected during the transient from regression analyses (as shown in Figure 2), the temperature-related error is reduced to 0.025 %, representing a 20-fold improvement over the traditional approach.

Stage 2: Temperature evolution after filling ($\dot{m}$ = 0)

The second stage is not required for the *RoR* mass flow rate calculation, but it enables determination of the steady-state gas temperature T_{ss} from pressure measurements. This stage begins when the inlet valve in **Figure 1** is closed, isolating the gas in the collection vessel.

With zero mass flow ($\dot{m}$ = 0), compression heating from flow work ceases, and the gas temperature gradually approaches the wall temperature T_w through radial conduction. During this thermal relaxation, the total gas mass (and therefore the gas density) remains constant, so changes in temperature drive a corresponding pressure relaxation. The pressure starts at its maximum value, corresponding to the full pressure P_{full}, and asymptotically approaches the equilibrium value, P_∞.

Because the volume-averaged density remains constant, the unknown steady-state temperature T_{ss} can be determined using the thermodynamic relationship,

$$\rho(P_{full}, T_{ss}) = \rho(P_\infty, T_w)\,, \qquad (13)$$

where, P_{full} is the measured pressure immediately after the valve is closed. This method is valid provided that the filling stage is sufficiently long for the gas to reach steady-state temperature T_{ss}.

Measuring the pressure trace during thermal relaxation enables determination of the thermal relaxation time constant τ, which characterizes the approach to equilibrium. During this process both the mass flow and thermal response factor are zero ($\dot{m}$ = 0, ε = 0), so Equation (10b) is

$$\tau\frac{dT}{dt} + T = T_w\,, \qquad (14a)$$

where the predicted thermal relaxation time is

$$\tau = \frac{m_{full}c_V}{8\pi kL}\,. \qquad (14b)$$

The solution for the gas temperature during relaxation is

$$T(t) = T_w + (T_{ss} - T_w)\exp\left(-\frac{t}{\tau}\right). \qquad (14c)$$

The corresponding pressure equilibration follows from the temperature relaxation through the real-gas equation of state,

$$P(t) = Z(\rho_{full}, T(t))\rho_{full}R_gT(t)\,, \qquad (15)$$

where the volume-averaged density at the end of filling ρ_{full} is defined in Equation (13).

Section 3.3 simplifies the analysis by assuming constant gas properties (c_V, k, ε). However, these properties vary slightly with pressure and temperature over the *RoR* operating range. To approximate this variation, one can use an average of the initial and final property values. Since the final temperature T_{ss} is unknown, an iterative solution is required.

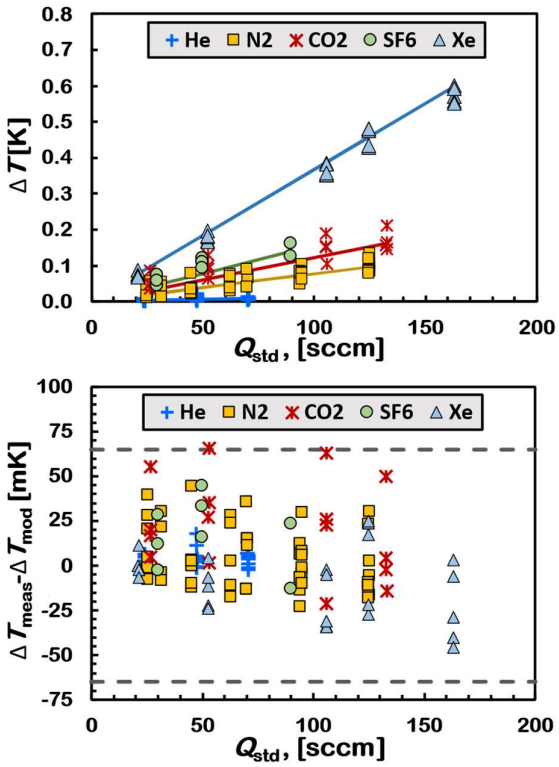

Figure 3. Comparison of measured and modeled temperature rises (ΔT) for five gases over a range of standard flow rates (Q_{std}). The upper panel shows absolute ΔT values for He, N_2, CO_2, SF_6, and Xe, with symbols for measured data and lines for modeled data. The lower panel plots the difference between measured and modeled ΔT to assess model accuracy, with ±65 mK bounds.

4. Results

We validated model predictions of the steady-state temperature increase ΔT_{model} across five gases (He, N_2, CO_2, SF_6, and Xe) and flow rates from 20 sccm to 163 sccm, as shown in **Figure 3**. This validation range focuses on the upper portion of the operating regime, where compression heating is most significant. The steady-state gas temperature T_{ss} was experimentally inferred using the pressure-based relaxation method, mathematically described in Section 3.3 and experimentally detailed in our previous work [5]. Following closure of the inlet valve in **Figure 1**, Equation (13) was applied using the measured pressures P_{full} and P_∞, together with the wall temperature T_w, to determine T_{ss} and the corresponding temperature increase due to flow work, $\Delta T = T_{ss} - T_w$.

The experimental measurements were performed using the two-tube collection vessel of SLowFlowS described in

Reference [5]. Its design is analogous to the *RoR* schematic shown in **Figure 1**, with an internal diameter $d = 1.143$ cm and total length $L = 3.66$ m. The vessel was originally designed to operate over a flow range from 0.01 sccm to 125 sccm. Operation at 125 sccm corresponds to the maximum design thermal response factor, $\varepsilon_{max} = 0.00153$, for xenon, the lowest-conductivity gas. The validation measurements extend to 163 sccm, exceeding the original design flow limit and providing a stringent test of the thermal model.

Figure 3 presents a comparison between the measured and modeled temperature increases (ΔT) of the five gases (He, N_2, CO_2, SF_6, and Xe) over a flow range of approximately 20 sccm to 163 sccm. The upper panel shows the absolute temperature increase as a function of gas flow. Measured data are represented with unique marker shapes for each gas, while the modeled data are shown with solid lines that match the color of the corresponding gas. The lower panel displays the difference between measured and modeled temperature increases ($\Delta T_{meas} - \Delta T_{model}$), highlighting the agreement and assessing the accuracy of the model.

In the upper panel, the temperature rise ΔT increases with flow rate for both measured and modeled data for all gases. Xenon exhibits the highest increase, with $\Delta T = 0.6$ K at the maximum flow of 163 sccm, due to its low thermal conductivity ($k_{Xe} = 0.00553$ W/(m K)). The other gases follow the same trend: gases with lower thermal conductivities exhibit larger temperature increases. Helium, which has a conductivity approximately 28 times that of xenon, shows a negligible temperature increase across the flow range tested. For each gas, the model closely follows the measured data, indicating good agreement across the entire flow range. This agreement demonstrates that the model reliably captures the thermal response of the gas during the flow process. The strong agreement between model and experiment suggests that the original design limit is conservative and supports extending the validated thermal response factor to $\varepsilon_{max} = 0.00199$ and flow to 163 sccm.

The lower panel provides a more quantitative view of the model's performance by plotting the difference between the measured and modeled temperature rises. The scatter in repeated calibration points across the flow range is attributed to the difficulty of measuring P_{full}, which must be recorded immediately after the inlet valve shown in **Figure 1** closes. The pressure transducer has a response time of approximately 20 ms, which limits its ability to accurately capture the true peak pressure at the exact moment the valve closes. As a result, small variations in the recorded P_{full} are believed to contribute to the observed scatter. Although the data exhibit a slight systematic bias of approximately 10 mK, nearly all temperature differences fall within the ±65 mK bounds indicated by the dashed lines. Assuming a rectangular distribution, the standard uncertainty is 65 mK/√3 (approximately 37.5 mK). The expanded uncertainty in the modeled temperature is $U(\Delta T_{model}) = 75$ mK. Given that we typically operate the *RoR* at wall temperatures of $T_w = 298.15$ K, the relative expanded uncertainty of the steady-state temperature is $U_r(T_{ss}) = 0.025$ %.

5. Discussion

The thermal model in this paper was validated using NIST's SLowFlowS two-tube *RoR* flow standard, which consists of two tubes connected in series by a U-bend, as illustrated in **Figure 1**. Table 1 lists the parameter values required to compute the thermal response factor ε using Equation (10c) for the five gases considered. The thermal response factor design limit identified in Section 4 is $\varepsilon_{Xe,max} = 0.00199$, which is set by xenon due to its low thermal conductivity. The corresponding design limit flow rate is $Q_{Xe,std} = 163$ sccm, strictly valid only for xenon. Other gases have thermal response factors below this limit ($\varepsilon < \varepsilon_{Xe,max}$), allowing the *RoR* to operate at flows above the 163 sccm design limit without compromising the accuracy of the thermal model.

Table 1. Thermal response parameters for the two-tube SLowFlowS collection vessel ($L = 3.66$ m, $d = 1.143$ cm) for flow $Q_{std} = 163$ sccm and gases He, N_2, CO_2, SF_6, and Xe. Thermodynamic and transport properties calculated using REFPROP [7].

Gas Type [ ]	$\varepsilon \times 10^{-3}$ [ ]	ΔT [mK]	T_{ss} [K]	$k \times 10^{-3}$ [W/(m·K)]	N_R [ ]
Xe	1.99	595	298.61	5.5	1.0050
SF_6	0.86	255	298.35	13.0	1.0142
CO_2	0.66	198	298.30	16.6	1.0066
N_2	0.43	127	298.25	25.8	1.0022
He	0.07	21.1	298.17	155.3	1.0004

For flows at which the standard volumetric flow rate Q_{std} would cause the thermal response factor ε to exceed $\varepsilon_{Xe,max}$, a longer collection vessel L can be used. If the flow per unit length (Q_{std}/L) is maintained equivalent to that of the original vessel, the thermal response factor remains unchanged for a given gas. NIST's SLowFlowS implements this strategy by using two collection vessels: a low-flow vessel consisting of two tubes in series with length $L = 3.66$ m and a high-flow vessel of sixteen tubes in series with $L = 29.26$ m [5]. Results in Section 4 demonstrated that the two-tube vessel can operate up to 163 sccm. Based on geometric scaling, the corresponding flow limit for the sixteen-tube vessel is 1304 sccm. Adopting these new flow limits increases the maximum flow limit in the two tubes from 125 sccm to 163 sccm and the sixteen tubes from 1000 sccm to 1304 sccm, respectively.

Instead of the series-based collection vessel illustrated in **Figure 1**, a parallel arrangement can be implemented to achieve the same temperature rise for a given gas, provided that Q_{std}/L (or equivalently $\dot{m}/L$) is constant. In a parallel configuration of N tubes all having the same length L_{tube}, ideally each tube carries the *same* fraction of the total mass flow, $\dot{m}_{tube} = \dot{m}_{total}/N$. In contrast, in the series configuration the total mass flow $\dot{m}_{total}$ resides in a single tube of length $L_{total} = N L_{tube}$. In both the series and parallel configurations, the mass flow per unit length is the same, $\dot{m}_{tube}/L_{tube} = \dot{m}_{total}/L_{total}$, ensuring the same thermal response factor ε for a specific gas.

Although series and parallel configurations can be designed to be thermally equivalent, they present different challenges for achieving low uncertainty flow measurements. Series configurations are conceptually robust because the gas experiences a single, well-defined thermal and mass-flow history. During filling, modest flow rates ($Q_{std} \leq 1000$ sccm) result in a nearly uniform pressure throughout the collection vessel. However, if the collection length is too long, the pressure relaxation method used to infer T_{ss} may no longer be viable. After closing the inlet valve, the time for pressure waves to travel from end to end is $2L_{total}/a_{sound}$, where L_{total} is the collection vessel length and a_{sound} is the speed of sound.

If the pressure wave travel time is comparable to or exceeds the system's thermal response time, pressure becomes an unreliable proxy for temperature, limiting the practical use of very long series tubes [5].

Thermally equivalent parallel configurations, on the other hand, have shorter tube lengths, avoiding pressure-relaxation issues. However, parallel arrangements require careful flow distribution and thermal isolation to ensure that each tube receives a nearly equal fraction of total mass flow rate, preserving the idealized thermal response factor. Additionally, the more complex tube arrangement in parallel configurations can lead to a higher pressure drop, especially if the flow distribution is not uniform.

Finally, it is important to distinguish between the geometric collection vessel length L and the effective thermal length L_{eff}, which governs ε in Equations (1) and (10c). The effective length L_{eff} represents the portion of the collection vessel where radial conduction to the wall is the dominant mechanism for removing compression-generated heat. In complex vessel designs, localized sections of the collection volume may experience other heat-transfer modes that fall outside the assumptions of the radial conduction model, so that L_{eff} is less than L. For example, in parallel configurations, the header connecting individual tubes may have a larger diameter, allowing natural convection to play a more substantial role in that region.

6. Conclusion

This study presents a novel collection vessel with an integrated thermal model that significantly improves the accuracy of mass flow rate measurements for multiple validated gas species gases (He, N_2, CO_2, SF_6, and Xe) using the Rate-of-Rise (*RoR*) method. The high-aspect-ratio, small-diameter (1.143 cm) vessel is designed with a low thermal response factor ($\varepsilon \ll 1$), ensuring that heat transfer is dominated by radial conduction, such that temperature rises are small and the temperature distribution is predictable. During filling, the gas temperature quickly approaches a steady-state temperature slightly above the measured wall temperature. Accurately predicting the gas temperature allows precise gas density calculations and, in turn, accurate determination of mass flow rate.

The reduced-order thermal model accurately predicts the volume-averaged gas temperature from exterior wall measurements. The experimentally validated temperature has a standard uncertainty of 37.5 mK across multiple gases and for flow rates from 20 sccm to 163 sccm. The validation work in xenon demonstrated that NIST's SLowFlowS two-tube vessel can operate up to 163 sccm. Thus, the proposed collection vessel design and thermal model facilitate accurate non-intrusive temperature determination for *RoR* standards and address limitations in temperature measurement accuracy in conventional *RoR* collection vessels, where heat transfer is often dominated by natural convection. Given excellent agreement between the model and measured data, we expect the model to perform well for any gas provided accurate thermodynamic and thermophysical properties are available.

The proposed collection vessel design is scalable with flow. For a given gas, shorter vessel designs can be extended to higher flow rates by increasing the vessel length while keeping the flow per unit length (Q_{std}/L) constant. This ensures that the thermal response factor (ε) remains unchanged. Consequently, both collection vessels are thermally equivalent, experiencing the same temperature increase due to flow work.

Series and parallel tube configurations with the same thermal response factor ε are thermally equivalent, exhibiting identical temperature transients and the same steady-state temperature. Practical tradeoffs between these two design strategies provide flexibility while maintaining predictable thermal behavior. The findings provide explicit design guidelines for future *RoR* standards, significantly reducing temperature-induced measurement uncertainty and enabling more reliable, reproducible characterization of mass flow controllers (MFCs) across gas species. These results have direct implications for industries such as semiconductor manufacturing, environmental monitoring, and precision instrumentation, where accurate calibration of MFCs across multiple gas species is critical for process quality and performance.

Future work will include computational investigations using CFD simulations to assess the impact of natural convection assumptions made in the conduction-only thermal model presented in this work, particularly at higher flow rates. Additionally, the influence of natural convection will be explored in more traditional collection vessel designs to further understand and refine the model's accuracy for a broader range of operating conditions.

References

[1] M. H. Kim, H. E. Sim, and S. J. Hong, "Part-Level Fault Classification of Mass Flow Controller Drift in Plasma Deposition Equipment," *IEEE Trans. Semicond. Manufact.*, vol. 37, no. 3, pp. 373–380, Aug. 2024, doi: 10.1109/TSM.2024.3396994.

[2] J. D. Wright, S.-I. Nakao, A. N. Johnson, and M. R. Moldover, "Gas flow standards and their uncertainty," *Metrologia*, vol. 60, no. 1, p. 015002, Feb. 2023, doi: 10.1088/1681-7575/ac8c99.

[3] J. D. Wright, A. N. Johnson, M. R. Moldover, and G. M. Kline, "Errors in rate of rise gas flow measurement from flow work," in *Proc. 10th Int. Symp. Fluid Flow*, Queretaro, Mexico, Mar. 2018.

[4] G. Zhang, B. Hui, Z. Xu, B. Zhou, B. Sundén, and Z. Cao, "A Review of Calibration Standards, Devices and Methods for Gas Flow in Semiconductor Manufacturing Processes," *Flow Measurement and Instrumentation*, vol. 101, p. 102753, Jan. 2025, doi: 10.1016/j.flowmeasinst.2024.102753.

[5] J. G. Pope, K. A. Gillis, A. N. Johnson, J. T. Boyd, and J. D. Wright, "SLowFlowS: A novel flow standard for semiconductor process gases," *Flow Measurement and Instrumentation*, vol. 102, p. 102831, Mar. 2025, doi: 10.1016/j.flowmeasinst.2025.102831.

[6] T. L. Bergman and A. S. Lavine, *Fundamentals of heat and mass transfer*, Eighth edition. Hoboken, NJ: John Wiley & Sons, 2017.

[7] M. Huber, A. Harvey, E. Lemmon, G. Hardin, I. Bell, and M. McLinden, "NIST Reference Fluid Thermodynamic and Transport Properties Database (REFPROP) Version 10 - SRD 23." National Institute of Standards and Technology, 2018. doi: 10.18434/T4/1502528.